Excitation factors for horizonless compact objects: long-lived modes, echoes, and greybody factors

Romeo Felice Rosato, ¹ Shauvik Biswas, ² Sumanta Chakraborty, ³ and Paolo Pani ¹

¹Dipartimento di Fisica, Sapienza Università di Roma & INFN, Sezione di Roma, Piazzale Aldo Moro 5, 00185, Roma, Italy ²Indian Institute of Technology, Gandhinagar, Gujarat 382055, India ³School of Physical Sciences, Indian Association for the Cultivation of Science, Kolkata 700032, India

We present an analytical and numerical investigation of the quasinormal excitation factors of ultracompact horizonless objects. These systems possess long-lived quasinormal modes with extremely small imaginary parts, originating from the effective cavity between the photon sphere and the object's interior. We show that the excitation of such modes is strongly suppressed, scaling with the imaginary part of their frequency, and therefore they contribute to the waveform only at very late times. This hierarchy naturally explains the structure of echo signals: the prompt ringdown is dominated by standard light-ring modes, the early echoes arise from moderately damped cavity modes, and only the latest echoes are governed by long-lived modes. Based on this, we propose a practical ringdown waveform model based on a superposition of ordinary black-hole quasinormal modes and cavity modes, which captures the complexity of the ringdown of horizonless ultracompact objects. We further demonstrate that the combination of small excitation factors and weak damping enhances the robustness of long-lived modes against localized perturbations, in contrast to the spectral instabilities affecting standard black-hole quasinormal modes. Finally, we extend the analysis of greybody factors to exotic compact objects and wormholes, showing that they remain stable under small deformations of the effective potential and thus represent robust observables. Our results provide a unified framework for understanding excitation, stability, and echoes in ultracompact horizonless objects, with direct implications for their spectral properties and gravitational-wave signatures.

CONTENTS

I.	Introduction	1
II.	Excitation factors of long-lived modes	2
III.	Echo reconstruction from the excitation factors of ECOs	6
IV.	Stability of long-lived modes	8
V.	Stability of Greybody factors	10
VI.	Conclusions	10
/II.	Acknowledgments	11
	References	12

I. INTRODUCTION

Black-hole (BH) perturbation theory [1, 2] is recently undergoing a phase of rapid advancement (see [3, 4] for recent reviews). This revival has been largely driven by the first gravitational-wave (GW) detections of remnant ringdowns [5–8] and by the prospect of BH spectroscopy [9–12] as a probe of gravity in the strong-field, dynamical regime [13–16].

The next decade promises a qualitative leap in precision, with current detectors reaching design sensitivity and with the advent of next-generation interferometers

such as LISA [17], Einstein Telescope [18–22], and Cosmic Explorer [23–25]. These facilities are expected to measure ringdowns at the sub-percent level [26–28], enabling unprecedented tests of General Relativity and of the nature of compact objects [16].

A central goal of BH spectroscopy is the extraction of multiple quasinormal modes (QNMs) [29–32] from the post-merger remnant as it approaches stationarity. In General Relativity, the entire QNM spectrum of a BH is uniquely determined by its mass and spin, allowing for stringent null-hypothesis tests of the theory [33, 34], of the remnant's nature [35–37], and of its surrounding environment [38–41]. The push toward accurate ringdown modeling has, however, uncovered additional layers of complexity, including environmental imprints [38, 42–46], modified boundary conditions or near-horizon structures [47–50], spectral instabilities [51–68], nonlinear effects [69–87], the role of overtones [88–90], and late-time tails [91–96].

In parallel with QNM-based analyses, an alternative line of investigation has emerged, focusing on BH greybody factors (GFs) [97–99]—real, frequency-dependent functions describing the tunneling probability through the BH effective potential [100]. GFs have been shown to capture the spectral amplitude of the ringdown at frequencies above the fundamental mode [97–99, 101], to remain robust under small deformations of the system, and to make contact with quantities that can be expressed as QNM superpositions, even in the presence of spectral instabilities [101, 102].

In this work we focus on the ringdown of ultracom-

pact, horizonless objects, often referred to as BH mimickers or exotic compact objects (ECOs) [16, 35, 36, 103]. It has been shown that, if the remnant is sufficiently compact [47–49], the prompt ringdown signal following the merger is universal, since it is governed by the local structure of the effective potential of null geodesics. Putative near-horizon structures, which can be modeled in terms of a reflectivity coefficient at the object's surface [104, 105], show up only at late times in the form of repeated and modulated GW echoes [47–49, 106]. The time delay between echoes depends on the compactness, while the relative amplitude of successive echoes encodes the reflectivity. Recently, it was further demonstrated that signals from ECOs also develop a late-time tail coinciding with that of BHs [96].

Several models of ECOs have been investigated over the years, including wormholes [107], constantreflectivity ECOs [35, 104, 105], and objects with Boltzmann reflectivity [108]. Here we provide an analytical and numerical characterization of the QNMs excitation for ECOs. Quasinormal excitation factors (QNEFs) [109-111] encode a universal, initialdata-independent measure of the relative excitation of QNMs, arising from the poles of the Green's function that propagates small perturbations of the geometry. QNEFs do not depend on the perturbation details; when combined with knowledge of the initial data they yield the quasinormal excitation coefficients, which quantify the actual QNM content of a waveform given a specific

To the best of our knowledge, this work presents the first attempt toward the computation of QNEFs for ECOs and BH mimickers. The QNM spectrum of such objects is characterized by the presence of long-lived modes, which arise because a horizonless object has a non-vanishing reflectivity, thereby creating an effective cavity between its interior and the gravitational effective potential barrier. We show that QNM excitation is strongly correlated with the small imaginary part of these mode: the smaller the damping, the weaker the excitation. This observation has significant implications for the physics of ECOs. In particular, it clarifies how cavity modes generate the sequence of echoes in the waveform. Long-lived modes have extremely small imaginary parts (i.e., nearly real frequencies), resulting in very weak excitation and contributing to the signal only at very late times, once all other modes have exponentially decaved. The cavity spectrum, however, is broader: it also contains modes with larger imaginary part than the long-lived branch, though still smaller than those of the Schwarzschild QNM spectrum. These modes are responsible for generating the first echoes observed after the prompt ringdown. This is discussed in detail in Sec. II, while in Sec. III we show how to reconstruct the echo signal from a superposition of QNMs with the corresponding excitation factors.

We also analyze the stability of the mode spectrum, which is intrinsically connected to the excitation factors. Indeed, an important feature of QNMs is their extreme sensitivity to small perturbations of the system [38, 51– 53, be them in the background geometry or in the boundary conditions. This suggests that the QNM spectrum of a BH could be drastically altered by environmental effects [38, 42–44] or near-horizon structures [47–50], although the prompt ringdown in the time domain is known to be far less affected [44, 47–49, 112, 113]. We investigate how wormholes and ECOs respond to such deformations [56, 114]. As discussed in Sec. IV, we find that long-lived modes are remarkably stable under small perturbations of the effective potential, providing an analytical understanding that is in agreement with some recent numerical results [114]. As we shall show, this robustness originates from the fact that the small imaginary part of the mode, together with the corresponding suppression of its excitation factor, prevents any significant amplification of the system's response.

As a corollary, in Sec. V we further verify that the GFs of wormholes and ECOs—recently demonstrated to be stable against small deformations of the effective gravitational potential for BHs [101, 102]—remain stable under analogous perturbations for these objects as well. This point is particularly relevant, as GFs play a crucial role in modeling the frequency-domain spectral amplitude of GWs for both ECOs and wormholes, as recently shown [115].

In the following, we use G = c = 1 units.

II. EXCITATION FACTORS OF LONG-LIVED MODES

For ultracompact objects, the fundamental quasinormal QNMs possess a very small imaginary part, corresponding to long-lived oscillations that remain quasitrapped between the object's interior and its photon sphere [116]. In the case of wormholes, this behavior arises due to the cavity formed between the two photon spheres on the two sides of the wormhole throat.

In this section, we examine the excitation factors associated with these long-lived QNMs for ultracompact, non-rotating objects [16, 36, 103]. We restrict to the non-rotating case and assume that the spacetime geometry outside the ultracompact object —or at least beyond an effective radius r_0 — is well described by the Schwarzschild metric. In both cases, the system is governed by the one-dimensional radial wave equation:

$$\left[\frac{d^2}{dr_*^2} + \omega^2 - V_l(r)\right] X_{lm\omega} = 0, \qquad (1)$$

where ω is the frequency of the perturbation, the tortoise coordinate r_* is defined via $dr/dr_* = 1 - 2M/r$, and M is the mass of the object. The function $X_{lm\omega}$ represents the radial part of the perturbation, which may be scalar, electromagnetic, or gravitational in nature, and $V_l(r)$ denotes the corresponding effective potential. For

gravitational perturbations, $V_l(r)$ corresponds to either the Regge-Wheeler or Zerilli potential, depending on the parity of the perturbation.

The eigenvalue problem associated with the secondorder differential equation (1) requires two boundary conditions: one at spatial infinity and the other at the inner boundary of the object, which depends on the specific model under consideration. QNMs require an outgoing boundary condition at infinity:

$$X_{lm\omega} \to e^{+i\omega r_*}; \quad r_* \to +\infty,$$
 (2)

where a time dependence of the form $e^{-i\omega t}$ is assumed for the perturbations, so that the positive (negative) exponential corresponds to an outgoing (ingoing) wave.

The inner boundary condition depends on the internal structure of the compact object and has to be discussed separately for each case. In general, it involves a superposition of outgoing and ingoing waves at the surface of the object, with the amplitude of the outgoing wave governed by the object's reflectivity.

In the following, we focus on two classes of ultracompact objects:

• Schwarzschild-like wormholes, modeled by joining two Regge-Wheeler¹ potentials at the origin. The effective potential in this case is given by [107, 117]

$$V_l(r_*) = \theta(r_* - r_*^0)W_l(r_*) + \theta(r_*^0 - r_*)W_l(-r_*), \quad (3)$$

with $W_l(r_*)$ being the Regge-Wheeler potential, and r_*^0 being the throat location in tortoise coordinates (while we shall denote the throat location in Schwarzschild coordinates as $r_{\text{throat}} = r(r_*^0)$).

• Schwarzschild-like reflecting ECOs, whose exterior geometry matches the Schwarzschild solution up to an effective radius r_0 . For ultracompact objects, the compactness condition $r_0 - 2M \ll M$ holds. For external observers, the ECO is modeled by the surface reflection amplitude $R_{\rm ECO}$ at its surface and its compactness $\epsilon = (r_0/2M) - 1$. These two parameters capture all the information about the linear response of the ECO interior [35, 104, 105]. Near this effective radius, the perturbing field behaves as [35, 104, 118],

$$\Psi \to e^{-i\omega(r_* - r_*^0)} + R_{\text{ECO}} e^{i\omega(r_* - r_*^0)}, \quad r_* \to r_*^0$$
 (4)

where $r_*^0 = r_*(r_0)$, the tortoise coordinate associated with the surface of the ECO.

The QNM problem can be regarded as a special case of the more general wave scattering problem, where the asymptotic behavior is

$$X_{lm\omega} \to A_{lm\omega}^{\text{in}} e^{-i\omega r_*} + A_{lm\omega}^{\text{out}} e^{+i\omega r_*}; \quad r_* \to +\infty.$$
 (5)

In particular, QNM frequencies correspond to the complex roots, $\omega_n = \omega_n^R + i\omega_n^I$, of the equation

$$A_{lm\omega}^{\rm in}\Big|_{\omega_n} = 0. \tag{6}$$

The boundary condition (5) also enables the definition of reflection and transmission amplitudes

$$R_{lm}(\omega) = \frac{A_{lm\omega}^{\text{out}}}{A_{lm\omega}^{\text{in}}}, \qquad T_{lm}(\omega) = \frac{1}{A_{lm\omega}^{\text{in}}}.$$
 (7)

From the above quantities one can compute the QNEFs, namely [110]

$$B_n = \frac{A_{lm\omega}^{\text{out}}}{2\omega_n \gamma_{lmn}}, \quad \text{with} \quad \gamma_{lmn} = \frac{dA_{lm\omega}^{\text{in}}}{d\omega} \bigg|_{\omega_n}, \quad (8)$$

where n identifies the overtone number. The QNEFs should not be confused with the quasinormal excitation coefficients, which instead depend on the specific source $I_{lm\omega}(r_*)$ entering the inhomogeneous version of Eq. (1), and are defined as [110]

$$C_n = B_n \int_{-\infty}^{+\infty} \frac{\psi_n(r_*) I_{lm\omega}(r_*) dr_*}{A_{lm\omega}^{\text{out}}}, \qquad (9)$$

where $\psi_n(r_*)$ denotes the solution of Eq. (1) corresponding to the specific *n*-th QNM. While the excitation factors B_n provide universal measures of QNM excitation, the coefficients C_n quantify the excitation of a given mode by a given source.

In the following sections we compute the QNEFs B_n both numerically and analytically. In the latter case the calculations are performed in the regime $|\omega|M \ll 1$, where Eq. (1) can be solved analytically [119]. Although restricted to this regime, these results provide useful insights into the general behavior of the QNEFs for the long-lived modes of wormholes and ECOs, while the full frequency range is addressed numerically.

We find it useful to introduce the cavity length, L. In the case of an ECO, where a partially reflecting surface is located at $r_* = r_*^0$, this length corresponds to the distance between the surface at $r_* = r_*^0$ and the peak of the gravitational potential at $r_* = r_*^{\max}$, namely $L = |r_*^0 - r_*^{\max}| \approx |r_*^0|$ (since for ultracompact objects the reflective surface lies at large negative tortoise coordinates compared to the maximum of the potential). In contrast, for a wormhole configuration, the cavity length corresponds to the distance between the two potential barriers.

Wormhole case. Using a transfer matrix approach [67], Ref. [115] demonstrates that, for wormholes, the ingoing wave amplitude $A_{lm\omega}^{\rm in}$ can be computed as

$$A_{lm\omega}^{\rm in} = \left(\alpha_{lm\omega}^{\rm in}\right)^2 e^{-i\omega L} - \left(\alpha_{lm\omega}^{\rm out,*}\right)^2 e^{i\omega L}, \qquad (10)$$

where L represents the effective length of the cavity, whereas $\alpha_{lm\omega}^{\rm in}$ and $\alpha_{lm\omega}^{\rm out}$ correspond to the standard ingo-

¹ For concreteness, we focus on gravitational axial perturbations; however, the analysis applies more generally.

ing and outgoing wave amplitudes in the BH case² [115]. In this case, Eq. (6) takes the form

$$e^{-2i\omega_n L} = \left(\frac{\alpha_{lm\omega_n}^{\text{out},*}}{\alpha_{lm\omega_n}^{\text{in}}}\right)^2 = e^{2\log\left(\frac{\alpha_{lm\omega_n}^{\text{out},*}}{\alpha_{lm\omega_n}^{\text{in}}}\right)} e^{-2\pi i n}, \quad n \in \mathbb{Z}.$$
(11)

The QNMs are therefore given by [120]

$$\omega_n = \omega_n^R + i\omega_n^I \sim \frac{\pi n}{L} + \frac{i}{L} \log \left(\frac{\alpha_{lm\omega_n}^{\text{out}}}{\alpha_{lm\omega_n}^{\text{in}}} \right), \qquad (12)$$

with $n \in \mathbb{Z}$. Note that long-lived modes appear in the low-frequency regime, in particular they are characterized by $|\omega_n^I| \ll |\omega_n^R| \ll M^{-1}$. In this limit, where the frequencies are approximately real, the ratio $\alpha_{lm\omega}^{\rm in}/\alpha_{lm\omega}^{\rm out}$ can be approximated as [119]

$$\left| \frac{\alpha_{lm\omega_n}^{\text{out}}}{\alpha_{lm\omega_n}^{\text{in}}} \right| = 1 - 2\beta_{ls} \left(2M\omega_n^R \right)^{2l+2} + \mathcal{O}\left(\left(M\omega_n^R \right)^{2l+4} \right) , \tag{13}$$

where $\beta_{sl} = \left(\frac{(l-s)!(l+s)!}{(2l)!(2l+1)!!}\right)^2$ and $s = (0, \pm 1, \pm 2)$ for scalar, electromagnetic, and gravitational perturbations, respectively. This leads to the expression [16]

$$\omega_n^I \sim -\frac{2\beta_{ls}}{L} \left(2M\omega_n^R\right)^{2l+2},$$
 (14)

which clearly satisfies our requirement $|\omega_n^I| \ll \omega_n^R$ for any n.

Now consider the following Taylor expansion for $A_{lm\omega}^{\rm in}$ around the QNM frequency ω_n ,

$$A_{lm\omega_n}^{\rm in} = \frac{dA_{lm\omega}^{\rm in}}{d\omega} \bigg|_{\omega} (\omega - \omega_n) + \mathcal{O}\left((\omega - \omega_n)^2\right). \quad (15)$$

Using Eq. (6) and the approximation (13), we find that, at $\omega = \omega_n$,

$$\frac{dA_{lm\omega}^{\text{in}}}{d\omega} \sim -2iL \left(\alpha_{lm\omega}^{\text{out},*}\right)^2 e^{i\omega_n L}, \qquad (16)$$

so that

$$\left| \frac{dA_{lm\omega}^{\text{in}}}{d\omega} \right| \sim 2L |\alpha_{lm\omega}^{\text{out}}|^2 = \frac{L}{2\beta_{ls}} \left(2M\omega_n^R \right)^{-2l-2} \,. \tag{17}$$

This yields

$$\left| \omega_n^I \frac{dA_{lm\omega}^{\text{in}}}{d\omega} \right|_{\omega_n} \sim 1 + \mathcal{O}\left((M\omega_n^R)^2 \right) . \tag{18}$$

We also need to compute the outgoing wave amplitude $A_{lm\omega}^{\rm out}$. Ref. [115] shows that, for wormholes,

$$A_{lm\omega}^{\text{out}} = \alpha_{lm\omega}^{\text{in}} \alpha_{lm\omega}^{\text{out}} e^{-i\omega L} - \alpha_{lm\omega}^{\text{in},*} \alpha_{lm\omega}^{\text{out},*} e^{i\omega L}.$$
 (19)

If one considers the squared absolute value of Eq. (19) and implements Eq. (6) for the wormhole case, it follows that

$$\left| A_{lm\omega}^{\text{out}} \right|^2 = \left(|\alpha_{lm\omega}^{\text{out}}|^2 - |\alpha_{lm\omega}^{\text{in}}|^2 \right)^2 , \qquad (20)$$

implying that $|A_{lm\omega_n}^{\text{out}}| = 1$ at the QNM frequency, since in the limit of nearly real frequencies it holds that $|\alpha_{lm\omega}^{\text{in}}|^2 - |\alpha_{lm\omega}^{\text{out}}|^2 = 1$ [115]. We can now compute the QNEFs B_n defined in Eq. (8) to be

$$|B_n| \sim \frac{|\omega_n^I|}{2|\omega_n|} \sim \beta_{ls} \frac{2M}{L} (2M\omega_n^R)^{2l+1},$$
 (21)

showing that the excitation factors satisfy $|B_n| \ll 1$ for long-lived modes, since they scale with ω_n^I . We stress that this result is valid only when $\omega_n^I \ll \omega_n^R < M^{-1}$. Nevertheless, it provides an interesting insight into how the QNEFs scale with the imaginary part of the relative QNM.

Equation (21) indicates that long-lived modes are only weakly excited during the ringdown phase. However, owing to their very small imaginary parts, they experience little damping and may eventually dominate the signal once the more strongly excited but shorter-lived modes have decayed. As a result, after the initial prompt ringdown, long-lived modes can re-emerge and produce so-called echoes (beatings of the cavity frequencies) with amplitudes much smaller than that of the initial signal.

The results presented in this section were verified numerically for gravitational perturbations in the wormhole scenario. In particular, Fig. 1 (upper left panel) displays the imaginary part of the first long-lived modes with l=2 as a function of the throat location $r_{\rm throat}$, while the upper right panel shows the corresponding derivative $dA_{lm\omega}^{\rm in}/d\omega$. Equation (18) holds in the regime $|\omega_n^I| \ll |\omega_n^R| \ll M^{-1}$, where our numerical computation is reliable; this agreement is clearly visible in the lower left panel of Fig. 1. Outside this regime, the approximation breaks down. The lower right panel shows the corresponding values of the QNEFs B_n .

ECO case. Using again a transfer matrix approach, Ref. [115] demonstrates that, for generic ECOs with surface reflectivity $R_{\rm ECO}$, the ingoing wave amplitude $A_{lm\omega}^{\rm in}$ can be computed as

$$A_{lm\omega}^{\rm in} = \alpha_{lm\omega}^{\rm in} e^{-2i\omega L} + \alpha_{lm\omega}^{\rm out,*} R_{\rm ECO} e^{2i\omega L}, \qquad (22)$$

implying

$$\omega_n = \frac{\pi n}{L} + \frac{i}{4L} \log \left(\frac{\alpha_{lm\omega_n}^{\text{out}}}{\alpha_{lm\omega_n}^{\text{in}}} R_{\text{ECO}} \right) \sim$$

$$\sim \frac{\pi n}{L} - \frac{i\beta_{ls}}{2L} \left(2M\omega_n^R \right)^{2l+2} + \frac{i}{4L} \log \left(|R_{\text{ECO}}| \right) . \quad (23)$$

² Namely, they correspond to the boundary conditions in Eq. (5) specialized to the BH case, where one simply replaces the symbol A with α in that equation.

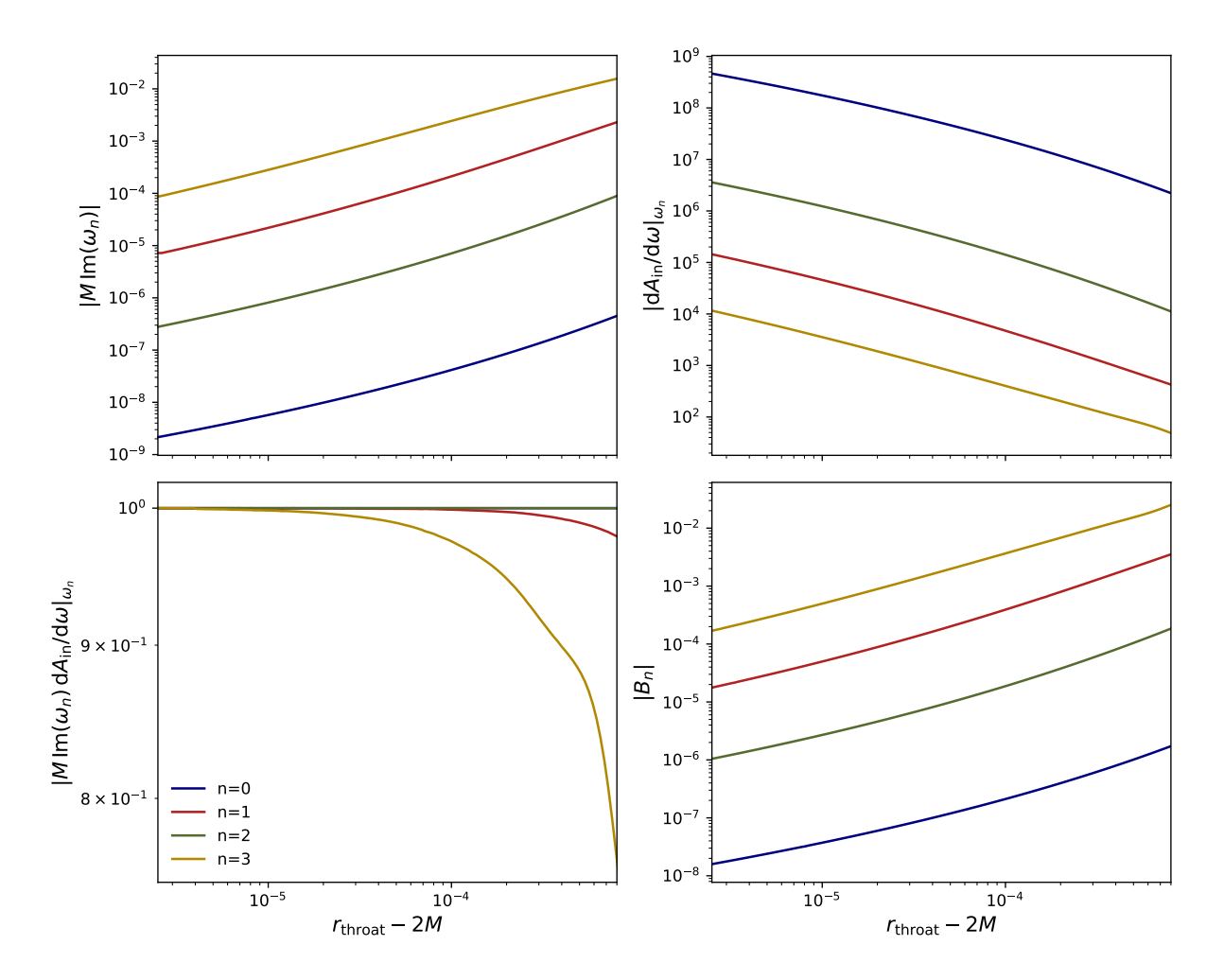


Figure 1. QNMs and excitation factors for axial gravitational perturbations with l=2 in the wormhole scenario. Top left panel: imaginary part of the first four long-lived modes, as a function of the throat location (horizontal axis). Top right panel: absolute value of $dA^{\rm in}/d\omega$ for the corresponding modes, using the same color coding. $dA^{\rm in}/d\omega$ becomes very large for long-lived modes, indicating that these modes are extremely suppressed (see Eq. (8)). Bottom left panel: the product $\omega_n^I dA^{\rm in}/d\omega$, which approaches unity when the throat location satisfies $\frac{(r_{\rm throat}-2M)}{2M} \ll 1$. This confirms the analytical predictions of Eq. (18). Bottom right panel: $|B_n|$ for the considered modes, using the same color coding. The QNEF is smaller for smaller imaginary part of the mode.

Hence, we obtain

$$\frac{dA_{lm\omega}^{\rm in}}{d\omega} \sim 4iL \,\alpha_{lm\omega}^{\rm out,*} R_{\rm ECO} e^{i\omega L} \,, \tag{24}$$

which corresponds to

$$\left| \frac{dA_{lm\omega}^{\text{in}}}{d\omega} \right| \sim \frac{2L}{\sqrt{\beta_{ls}}} \left(2M\omega_n^R \right)^{-l-1} |R_{\text{ECO}}|.$$
 (25)

We also need to compute $A^{\rm out}_{lm\omega}$, that for generic ECOs reads [115]

$$A_{lm\omega}^{\text{out}} = \alpha_{lm\omega}^{\text{out}} e^{-2i\omega L} + \left(\frac{1}{\alpha_{lm\omega}^{\text{in}}} + \frac{\alpha_{lm\omega}^{\text{out}} \alpha_{lm\omega}^{\text{out,*}}}{\alpha_{lm\omega}^{\text{in}}}\right) R_{\text{ECO}} e^{2i\omega L}.$$
(26)

By substituting it into Eq. (6) evaluated in the ECO case,

we obtain

$$|A_{lm\omega}^{\text{out}}| = \left| \frac{R_{\text{ECO}}}{\alpha_{lm\omega}^{\text{in}}} e^{2i\omega L} \right| \sim \frac{2\sqrt{\beta_{ls}}|R_{\text{ECO}}|}{(2M\omega_n^R)^{-l-1}}.$$
 (27)

This yields again a suppressed excitation factor:

$$|B_n| \sim \beta_{ls} \frac{M}{L} \left(2M\omega_n^R\right)^{2l+1}$$
 (28)

Indeed, long-lived modes arise again in the regime $\omega_n^I \ll \omega_n^R \ll M^{-1}$, which leads to small QNEFs. The above discussion demonstrates that the weak excitation of long-lived modes is a universal feature of ECOs as well as wormholes.

The results presented in this section have been numerically validated for gravitational perturbations in the context of different ECO models, in particular a Boltzmann

reflectivity ECO [108] and configurations with constant reflectivity. Specifically, Fig. 2 shows the behavior of the imaginary part of the first long-lived modes for l=2 as a function of the object's radius r_0 in the upper panel. In the middle panel the corresponding $\mathrm{d}A^{\mathrm{in}}_{lm\omega}/\mathrm{d}\omega$ are showed, while in the bottom panel we show the corresponding B_n .

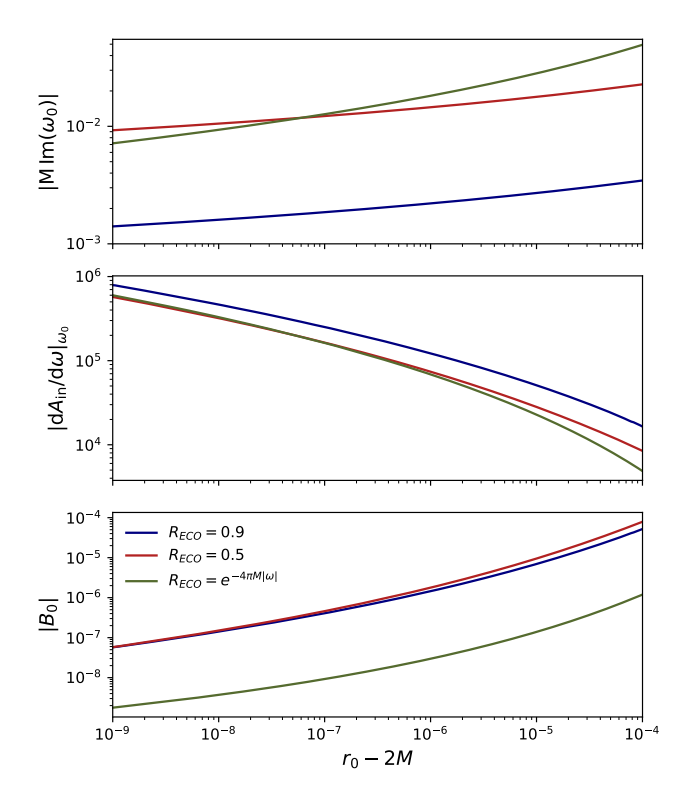


Figure 2. All panels refer to the l=2 mode of a gravitational perturbation for different ECO scenarios. Top panel: imaginary part of the fundamental long-lived quasinormal mode for gravitational perturbations as a function of the object's radius r_0 , for three different ECO reflectivities: constant reflectivity with $R_{\rm ECO}=0.9$, $R_{\rm ECO}=0.5$, and a Boltzmann reflectivity profile. Middle panel: corresponding behavior of the absolute value of the $dA^{\rm in}/d\omega$ for the same modes and models. Again, for long-lived modes the derivative $\frac{dA^{\rm in}_0}{d\omega}$ is large, which implies that the corresponding modes are only weakly excited. Bottom panel: the corresponding values of the QNEFs B_0 for the cases under consideration.

III. ECHO RECONSTRUCTION FROM THE EXCITATION FACTORS OF ECOS

In this section we will show how to reconstruct the ECO response from the QNEFs. To this purpose, it is instructive to compute the Fourier transform of the reflectivity, namely

$$\mathcal{R}_{lm}(t) = \frac{1}{2\pi} \int_{-\infty}^{+\infty} d\omega R_{lm} e^{-i\omega t} , \qquad (29)$$

as this quantity captures the spectral content of the reflected signal. In particular, following Ref. [101], the reflectivity can be evaluated either directly or by analyzing the analytic structure of the ingoing amplitude in the complex frequency plane [109]. The dominant contribution comes from the simple poles located at the QNM frequencies, corresponding to the complex roots of the ingoing amplitude. Applying the residue theorem, one obtains

$$\mathcal{R}_{lm}(t) \approx 4 \operatorname{Re} \left[\sum_{n=1}^{n_{\max}} \omega_n B_n e^{-i\omega_n t} \right],$$
 (30)

where the dependence of ω_n and B_n on (l, m) is left implicit. Within this framework, it becomes clear that the magnitude of the QNEFs, B_n , plays a fundamental role in understanding the echo signal. As previously discussed, the QNM spectrum of horizonless ultracompact objects is characterized by a set of modes with small imaginary part, arising because of the presence of an effective cavity in the potential. Among these cavity modes, longlived modes correspond to a subset with particularly small imaginary part. However, all cavity modes feature small imaginary parts (smaller than those of standard BH QNMs, for reference). As shown by the analytical results of the previous section, this implies that cavity modes are generally weakly excited (e.g., when compared to the QNMs of a standard BH). Nevertheless, their small imaginary parts also make them only weakly damped over time, so that they decay appreciably only on long timescales. The excitation coefficients B_n determine which of these modes dominate the signal at different stages of the evolution.

Importantly, the early ringdown of wormholes and ECOs is identical to that of a standard BH with the same mass at early times [47, 48, 121]. In Ref. [115], it was shown that the reflectivity in the frequency domain exhibits oscillatory features. The same work demonstrated that, by isolating the high-frequency oscillations of the reflectivity and performing a Fourier transform, one can reconstruct the late-time echoes in the time domain. This was achieved by gluing the reflectivity of a non-rotating wormhole to that of a reference Schwarzschild BH with the same mass. The matching was performed at a reference frequency $\omega_{\rm ref} = \sqrt{V_{\rm max}}$ (where $V_{\rm max}$ is the peak of the effective potential for the perturbation under consideration): at low frequencies, the contribution corresponds to that of a fictitious BH with the same mass as the wormhole, whereas at high frequencies the exact wormhole reflectivity is used. This construction enforces that the prompt ringdown of wormholes and ECOs coincides with that of a standard BH, while the first echoes arise predominantly from high-frequency features of the reflectivity.

Here, we extend this methodology to QNMs, proposing a framework to reconstruct the time-domain signal of horizonless ultracompact objects. In principle, by retaining a sufficiently large set of ECO oscillation modes, one could reproduce the entire ringdown, echoes included

³. In practice, however, this would require a very large number of modes (typically tens to hundreds) [122] rendering such an approach phenomenologically impractical. Therefore, along the lines of [115], here we show that it is possible to proceed by modeling the early ringdown phase using standard BH QNMs, and the echo signal using only the oscillation frequencies of the cavity. In practice, we use the following reconstruction

$$\mathcal{R}_{lm}(t) \approx \theta(2L - t) \, 4\text{Re} \left[\sum_{n=1}^{n_{\text{max}}} \omega_n^{\text{BH}} B_n^{\text{BH}} e^{-i\omega_n^{\text{BH}} t} \right]$$

$$+ \theta(t - 2L) \, 4\text{Re} \left[\sum_{n=1}^{n_{\text{max}}} \omega_n^{\text{cavity}} B_n^{\text{cavity}} e^{-i\omega_n^{\text{cavity}} t} \right], \quad (31)$$

where the suffix indicates if the considered QNMs and QNEFs are associated to either BH or cavity modes, and L is the cavity length. The resulting time-domain signal reproduces the waveform, as shown in Fig. 3 for the wormhole scenario, with high accuracy. We stress that this framework is purely phenomenological, since BH QNMs are not part of the ECO spectrum.

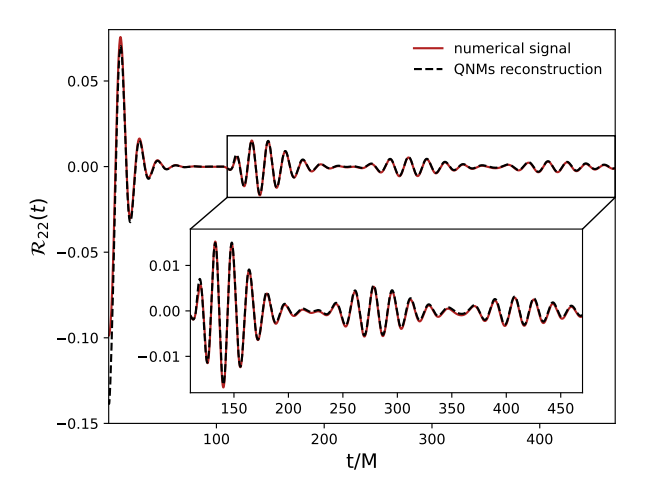


Figure 3. Fourier transform of the reflectivity for a wormhole with throat location $r_{\rm throat} = (2+10^{-6})M$. To reconstruct the time-domain signal, we employ Eq. (31), with $n_{\rm max}^{\rm BH} = 7$ for BH QNMs and $n_{\rm max}^{\rm cavity} = 12$ for cavity modes. Here the cavity length crresponds to $L \sim 54M$. The resulting waveform accurately reproduces the oscillatory structure of the signal.

Our aim now is to gain a deeper understanding of the structure of echoes. In Fig. 3 we employed a large number of modes in Eq. (31) to reproduce the time-domain signal. It is worth emphasizing that, in this theoretical

analysis, no fitting procedure is involved: we simply compare a numerical time-domain result with its analytical counterpart given by Eq. (31). However, in a realistic data-analysis context, where one attempts to fit observational data using theoretical QNMs, employing too many modes is not viable, as it may lead to overfitting issues [90]. Later on, we will show that such a large number of modes is in fact unnecessary.

Up to now, we have discussed that the wormhole/ECO signal can be interpreted as consisting of two distinct stages:

- Early ringdown. As phenomenologically shown, this stage can be accurately reproduced using the modes of a fictitious BH with the same mass as the wormhole or ECO. As known from the BH case, only a few modes are sufficient to obtain a good reconstruction of the signal.
- Echoes stage. This phase is seeded by the cavity modes, which manifest as beat-like oscillations resulting from the interference between the trapped modes within the effective cavity.

However, the contribution of cavity modes to echoes is not the same at every stage. In particular, one must understand *how* cavity modes contribute. Indeed, the excitation of these modes scales with ω_n^I , as previously shown.

Echoes are typically associated with the long-lived modes, which however constitute only a limited portion of the cavity-mode spectrum. Here, the first key point we wish to emphasize is that the echoes are not produced solely by the long-lived modes; rather, they are generated by the entire set of cavity modes, which is larger than the subset of long-lived modes. In particular, as we have shown, the longer-lived a mode is (i.e. the smaller its imaginary part in absolute value), the more strongly its excitation factor is suppressed. For this reason, we do not expect the long-lived modes to contribute significantly to the first echoes, which have the largest amplitudes.

In Fig. 4 we display a representative portion of the spectrum of cavity modes for a specific wormhole configuration with $r_{\text{throat}} = 2M(1+10^{-7})$. To disentangle the role of the long-lived modes, we introduce a reference frequency corresponding to $\omega_{\rm ref} \sim \sqrt{V_{\rm max}}$, following Ref. [115], where V_{max} is the peak of the effective potential for the perturbation under consideration (axial gravitational ones, in this example). Long-lived modes lie below this reference frequency, as shown in the left panel of the figure. In the right panel, the black solid line represents the echo portion of the numerical timedomain reflectivity. We then attempt to reconstruct the signal by (i) including only the modes with real parts below the reference frequency (light-blue dashed line), and (ii) including all cavity modes (orange dashed line). As can be deduced from Fig. 4, the modes with extremely small imaginary parts contribute predominantly to verylate-time echoes, but not to the first echoes of the signal.

³ A related discussion in a different but conceptually equivalent framework is given in Ref. [122].

Indeed, in the figure the light-blue dashed line reproduces the last echo more accurately than the first two, though not perfectly.

From a phenomenological perspective, however, the first echoes are the most relevant ones. These are instead governed by modes with larger imaginary parts, which typically also have larger real parts compared to those of the long-lived branch, namely $\omega_R > \omega_R^{\rm BH} \sim \sqrt{V_{\rm max}}$. This behavior is fully consistent with our previous finding that early echoes are driven by the high-frequency features of the system [115]. As illustrated in the right panel of Fig. 4, when high-frequency modes are included, the echoes are faithfully reconstructed. If they are excluded, the echo structure is lost.

Minimal waveform for BH ringdown+echoes. We have therefore demonstrated that high-frequency cavity modes dominate the formation of the first echoes in the ringdown of horizonless ultracompact objects. However, in the previous reconstruction we still employed a large number of modes. The next question we address is: how many of these high-frequency cavity modes are actually needed to reconstruct the echoes? Our second key result is that only a few such modes are sufficient. In general, only a small number of modes (between 2 and 4) is required to reconstruct a single echo. In Fig. 5, we show the case of an echo in the wormhole signal with throat location at $r_{\text{throat}} = 2.0001M$. Already two modes (dashed blue line) provide a qualitatively good reconstruction of the numerical signal (black solid line), while four modes (dashed orange line) further improve the agreement, leading to a satisfactory reproduction of the entire echo struc-

Based on the above findings, we propose a phenomenological ringdown waveform

$$h(t) = \theta(2L - t) \sum_{lmn} A_{lmn} \cos\left(\omega_{lmn}^R t + \phi_{lmn}\right) e^{\omega_{lmn}^I t}$$

$$+ \theta(t - 2L) \sum_{lmn} \hat{A}_{lmn} \cos\left(\hat{\omega}_{lmn}^R t + \hat{\phi}_{lmn}\right) e^{\hat{\omega}_{lmn}^I t},$$
(32)

where A_{lmn} and ϕ_{lmn} denote the amplitude and phase of the (l, m, n) BH mode, with (l, m, n) being the angular, azimuthal, and overtone number, respectively. The corresponding hatted quantities refer instead to cavity modes.

The first line of Eq. (32) is the usual BH ringdown waveform truncated at t=2L, while the second line implements the echo reconstruction with the cavity modes previously discussed. This phenomenological model is similar in spirit to the QNM superposition studied in Ref. [123], but informed by the cavity modes.

Compared to a standard ringdown waveform, the model above has 4N extra parameters when N cavity modes are considered. Indeed, each mode is described by the amplitude, phase, frequency, and damping time; one of the phases must be fixed to require continuity of the waveform at t=2L, but this is compensated by the

extra L parameter. For example, considering two cavity modes only, one would need to include 8 extra parameters. A given ECO model would fix all the cavity QNMs in terms of ϵ , effectively reducing the number of extra parameters to 2N+1.

IV. STABILITY OF LONG-LIVED MODES

It is well established that QNMs are highly sensitive to small perturbations of the system [51–53], whether these affect the background geometry or the boundary conditions. This strong sensitivity implies that the QNM spectrum of a BH can be significantly distorted in the presence of environmental effects [38, 42–44] or any structure near the horizon [47–50]. Nevertheless, the early-time ringdown signal in the time domain is generally much less susceptible to such modifications [44, 47–49, 112, 113].

Here we given an analytical argument showing that, for ECOs and wormholes, the long-lived QNMs are remarkably robust against localized perturbations of small amplitude, as recently found numerically [114]. In particular, modes with smaller imaginary parts tend to be more stable. To demonstrate this, let us consider the wave equation (1). We model the perturbation of the potential as a localized deformation of amplitude $\epsilon V_{\text{bump}}(r_*)$, with $\epsilon \ll 1$. Provided that the transfer matrix approximation holds [67], and placing the bump to the right of the unperturbed potential $V_l(r_*)$ (without loss of generality), the scattering problem can be described as [67]:

$$\psi(r_* = +\infty) = \mathcal{M}_{\text{bump}} U(c) \,\mathcal{M}_0 \,\psi(r_* = -\infty) \,, \quad (33)$$

where \mathcal{M}_0 and $\mathcal{M}_{\text{bump}}$ are the transfer matrices corresponding to the background potential and the bump respectively, U(c) is a translation operator by a distance c, representing the position of the bump.

The total transmission coefficient of the system is given by

$$\frac{1}{T_{\text{tot}}} = -\frac{R'_{\text{bump}}R_0}{T_{\text{bump}}T_0}e^{i\omega c} + \frac{1}{T_{\text{bump}}T_0}e^{-i\omega c} = e^{-i\omega c} \left(A_0^{\text{in}}A_{\text{bump}}^{\text{in}} - A_0^{\text{out}}A_{\text{bump}}^{\prime\text{out}}e^{2i\omega c}\right), \quad (34)$$

and QNMs correspond to the roots of Eq. (34).

Perturbative analysis around a long-lived mode. We now focus on a long-lived QNM of the unperturbed system, characterized by a frequency ω_n with small imaginary part. For frequencies $M\omega > \epsilon$, the outgoing amplitude associated with the bump is strongly suppressed, while the ingoing amplitude approaches unity. Specifically, we can write

$$A_{\rm bump}^{\prime {\rm out}} \sim \epsilon \, a(\omega) \,, \qquad A_{\rm bump}^{\rm in} \sim e^{i\delta} - \epsilon \, b(\omega) \,, \qquad (35)$$

where $a(\omega)$ and $b(\omega)$ are finite complex functions of the frequency, and $\delta \in \mathbb{R}$ is a phase shift.

Near the unperturbed QNM frequency ω_n , we can expand the ingoing amplitude of the background system

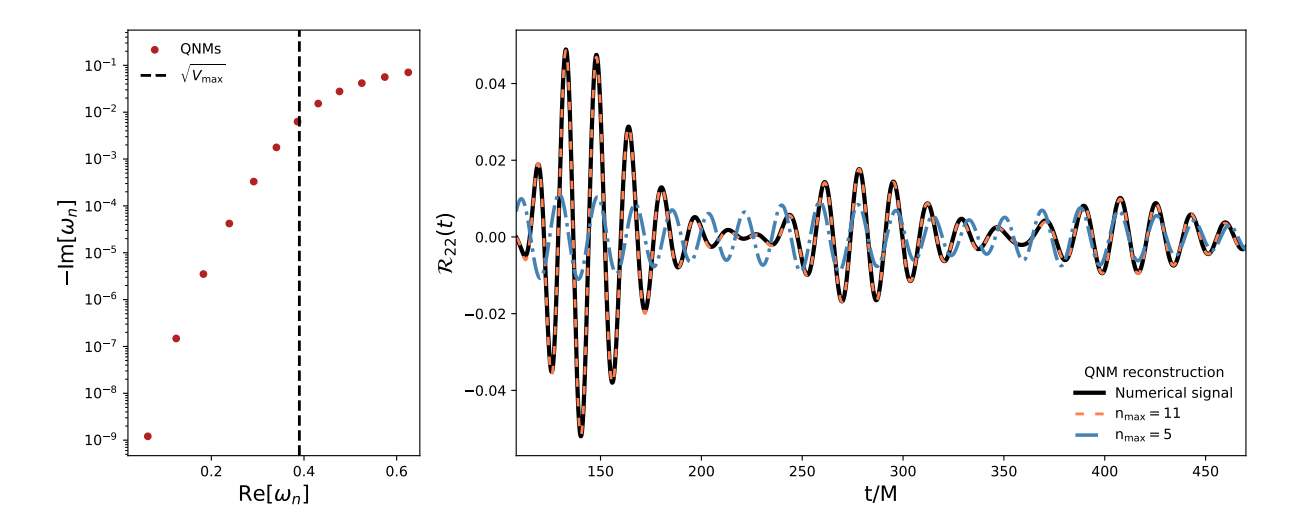


Figure 4. Mode content and echo reconstruction for a wormhole with throat location at $r_{\rm throat} = (2+10^{-6}) M$ Left: representative portion of the cavity-mode spectrum. The longest-lived modes do not dominate the echo onset because their excitation factors are highly suppressed. Right: comparison between the numerical echo signal and QNM-based reconstructions with/without high-frequency modes (defined as those with $\omega_n^R > \sqrt{V_{\rm max}}$). Including high-frequency modes yields an accurate reconstruction of the first echoes; excluding them reproduces only very-late-time echoes.

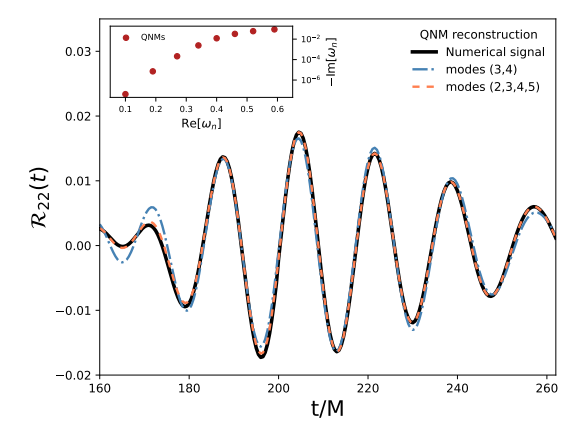


Figure 5. Reconstruction of a wormhole echo with throat location $r_{\rm throat}=2.00001M$. The inset in the upper left shows a representative set of QNMs. The numerical signal is shown as a black solid line, focusing on the second echoes in the interval 4L < t < 6L. The dashed blue line corresponds to a reconstruction with two modes, specifically the fourth and fifth ones, i.e. the first two modes above the threshold $\sqrt{V_{\rm max}}$, which already provide a good agreement. The dashed orange line shows the case with four modes, yielding an even better match. This demonstrates that only a small number of modes is sufficient to reproduce the echo.

as

$$A_0^{\rm in}(\omega) \simeq \left. \frac{dA_0^{\rm in}}{d\omega} \right|_{\omega_n} (\omega - \omega_n).$$
 (36)

Substituting into Eq. (34), and normalizing $A_0^{\text{out}} = 1$, we

obtain

$$\frac{dA_0^{\text{in}}}{d\omega}\Big|_{\omega_n} (\omega - \omega_n) \left(e^{i\delta} - \epsilon b(\omega)\right) - \epsilon a(\omega)e^{2i\omega c} = 0.$$
 (37)

This equation can be solved perturbatively by setting $\omega = \omega_n + \Delta\omega_n$, which yields

$$\Delta\omega_n = 2\epsilon\omega_n e^{-i\delta + 2i\omega_n c} a(\omega_n) B_n , \qquad (38)$$

where, interestingly, the QNEF B_n also appear naturally in this context.

Implications for mode stability. Eq. (38) shows that the frequency shift $\Delta\omega_n$ remains of order $\mathcal{O}(\epsilon)$ as long as the condition $2c < 1/|\mathrm{Im}(\omega_n)|$ is satisfied. However, when $2c > 1/|\mathrm{Im}(\omega_n)|$, the correction grows exponentially with c, signaling a potential instability. Therefore, modes with a larger imaginary part (i.e., shorterlived) are more susceptible to instability, while long-lived modes exhibit enhanced stability under local perturbations.

Furthermore, $\Delta\omega_n$ for long-lived QNMs is further suppressed due to the small value of the QNEF B_n , which scales as $\sim |\omega_n^I|$, as previously discussed.

Numerical verification. To support the analytical findings above, we will now numerically investigate the effect of small perturbations by modifying the effective potential V_l as follows

$$V_{\text{eff}}(r_*) = V_l(r_*) + \frac{\epsilon}{M^2} \operatorname{Sech}(r_* - c)^2.$$
 (39)

In the case of a symmetric wormhole geometry, we preserve the mirror symmetry by applying the same perturbation in both universes, placing it symmetrically with respect to the throat location r_0 , as done in the standard configuration.

Figure 6 illustrates the response of the system to the localized perturbation (39), comparing three representative QNMs: a standard (rapidly damped) mode, a longlived mode, and an intermediate (cavity) mode. The left panel shows the relative change of ω_n^R as a function of the bump location c/M, while the right panel reports the relative change of ω_n^I . For the data shown we set the bump amplitude to $\epsilon=10^{-4}$ (the magnitude of the perturbation can be estimated as $\epsilon/(M^2V_{\rm max}) \simeq 6.64 \times 10^{-4}$). The plotted complex frequencies are: standard mode $M\omega_{\rm standard} = 0.590 - 0.0894i$ (blue), long-lived mode $M\omega_{\rm long} = 0.189 - 7.086 \times 10^{-6} i$ (red), and intermediate (cavity) mode $M\omega_{\rm int} = 0.401 - 0.012 i$ (green). The three modes display markedly different behavior: the standard mode is strongly destabilized, with relative shifts that rapidly exceed the perturbation scale $\mathcal{O}(\epsilon)$. By contrast, the long-lived mode is essentially unaffected, its real part shifting by orders of magnitude less than ϵ and its imaginary part changing at most by a factor of order unity. The intermediate (cavity) mode exhibits an intermediate response. Consistently with Eq. (38), its relative variation begins to exceed the perturbative magnitude for $c \sim 1/|\operatorname{Im}\omega|_{\operatorname{int}} \simeq 83M$, and the exponential growth predicted by Eq. (38) is visible over the displayed range of c/M.

V. STABILITY OF GREYBODY FACTORS

Recent work has investigated the stability of GFs under small perturbations of the system, as well as their connection with observable quantities [98, 99, 101, 102]. In particular, by considering the modification introduced in Eq. (39) and recalling that the GF is a function of frequency, we can quantify the corresponding variation through the relative difference

$$\mathcal{G}_{lm} = \frac{\int_0^\infty |\Gamma_{lm}^{\epsilon}(\omega, c) - \Gamma_{lm}(\omega)| \ d\omega}{\int_0^\infty \Gamma_{lm}(\omega) \ d\omega}, \tag{40}$$

where the unperturbed greybody factors $\Gamma_{lm}(\omega)$ and the perturbed ones $\Gamma_{lm}^{\epsilon}(\omega,c)$ are computed via direct numerical integration, employing high-order analytic series expansions to ensure high precision [124, 125].

This variation is illustrated in Fig. 7. The left panel shows the case of wormholes for different values of ϵ , where the variation never exceeds the order of magnitude of the corresponding perturbation. The right panel presents the results for different ECO configurations, namely: constant reflectivity with $R_{\rm ECO}=0.9$ (green solid line), $R_{\rm ECO}=0.5$ (red solid line), and a Boltzmann reflectivity profile (blue solid line). In all cases, the variation remains bounded within $\mathcal{O}(\epsilon)$, confirming that both wormhole and ECO greybody factors are stable under small perturbations.

VI. CONCLUSIONS

In this work, we investigated the QNEFs and their connection to the ringdown of ultracompact horizonless objects. Using models such as Schwarzschild-like wormholes and partially absorbing ECOs, we systematically analyzed the excitation of their quasinormal spectra. Our results highlight several noteworthy features of QNEFs and their relevance to the physics of ultracompact objects.

First, we showed that long-lived QNMs (such as the cavity modes), which characterize the spectra of these systems, are only weakly excited during the ringdown. This observation has several implications: it explains why long-lived modes appear only at late times in the waveform, producing echoes. Since they are weakly excited, they do not affect the prompt ringdown, which remains dominated by standard BH (i.e., photon-sphere) modes. They become visible only after the standard QNMs have decayed, and —being associated with cavity modes— give rise to echoes as interference patterns. Moreover, the long-lived QNEFs scale as $\sim |\omega_n^I|$, implying that higher-frequency modes (with larger absolute imaginary parts) contribute earlier in the signal, whereas the low-frequency part of the spectrum manifests only at very late times.

Based on this result, we proposed a practical ringdown waveform model (Eq. (32)) based on a superposition of ordinary BH QNMs at early time and cavity modes at later times, which captures the whole complexity of the ringdown of horizonless ultracompact objects with a minimal set of waveform parameters.

A second key result is that the combination of small QNEFs and small imaginary parts prevents long-lived modes from becoming spectrally unstable, as we demonstrated analytically.

Finally, we extended previous analyses of the stability of GFs to ECOs and wormholes, showing that GFs constitute robust observables even for horizonless ultracompact objects.

The present work opens several directions for future research. A natural extension is the generalization of our analysis to *rotating* geometries, where both the structure of the effective potential and mode pattern become significantly richer. Another promising direction concerns the connection between QNEFs and the time-domain response in more realistic scenarios, e.g. in a particle infall experiment where the specification of the source allow us to compute the corresponding excitation coefficients. Finally, it would be interesting to devise search strategies based on our ringdown+echo waveform model, which captures the standard prompt BH ringdown and the first few echoes with a minimal set of parameters.

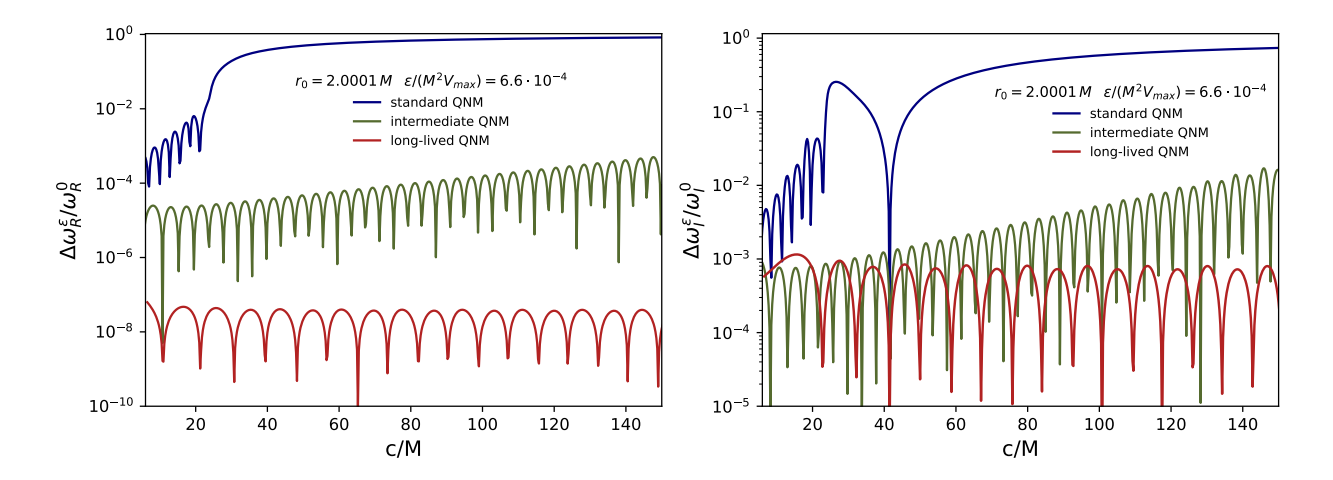


Figure 6. Response of three QNMs to the localized perturbation in Eq. (39) with $\epsilon = 10^{-4}$ for a wormhole with throat $r_0 = 2.0001M$. Left: relative change of Re ω as a function of c/M. Right: relative change of Im ω as a function of c/M. The curves correspond to: a standard (rapidly damped) QNM (blue solid line) whose imaginary part is comparable with the one of Schwarzschild fundamental mode, $M\omega_{\rm standard} = 0.590 - 0.0894\,i$; a long-lived mode (red solid line) with $M\omega_{\rm long} = 0.189 - 7.086 \times 10^{-6}\,i$; an intermediate cavity mode (green solid line), with $M\omega_{\rm int} = 0.401 - 0.012\,i$, whose damping rate lies between that of the Schwarzschild fundamental mode and that of the long-lived mode. The standard mode is strongly destabilized, whereas the long-lived mode remains essentially unaffected. The intermediate mode shows intermediate behavior. See the main text for quantitative details.

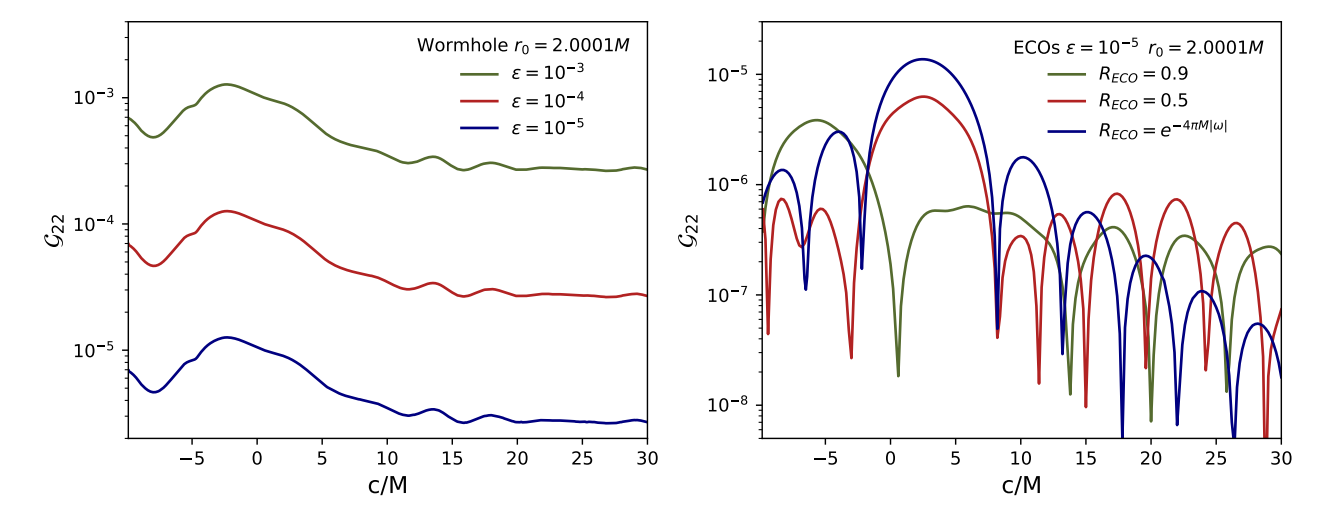


Figure 7. Relative variation \mathcal{G}_{lm} of the greybody factors under a localized perturbation of the effective potential, as introduced in Eq. (39), shown as a function of its location c/M and defined in Eq. (40). Left panel: wormhole case for different values of the perturbation amplitude ϵ . The variation remains consistently within the same order of magnitude as the perturbation. Right panel: results for three different ECO models — constant reflectivity with $R_{\rm ECO} = 0.9$ (green), $R_{\rm ECO} = 0.5$ (red), and a Boltzmann reflectivity profile (blue). In all cases, the deviation does not exceed $\mathcal{O}(\epsilon)$, confirming the stability of the GFs.

VII. ACKNOWLEDGMENTS

This work is partially supported by the MUR FIS2 Advanced Grant ET-NOW (CUP: B53C25001080001) and by the INFN TEONGRAV initiative. SB thank PhD fellowship provided by IACS, as a part of this work was done when he was a PhD student there.

- T. Regge and J. A. Wheeler, Phys. Rev. 108, 1063 (1957).
- [2] S. Chandrasekhar, The mathematical theory of black holes (1985).
- [3] E. Berti et al., (2025), arXiv:2505.23895 [gr-qc].
- [4] G. Carullo, Gen. Rel. Grav. 57, 76 (2025).
- [5] B. P. Abbott et al. (LIGO Scientific, Virgo), Phys. Rev. Lett. 116, 061102 (2016), arXiv:1602.03837 [gr-qc].
- [6] R. Abbott et al. (LIGO Scientific, Virgo), Phys. Rev. Lett. 125, 101102 (2020), arXiv:2009.01075 [gr-qc].
- [7] A. G. Abac et al. (LIGO Scientific, KAGRA, Virgo), Phys. Rev. Lett. 135, 111403 (2025), arXiv:2509.08054 [gr-qc].
- [8] (2025), arXiv:2509.08099 [gr-qc].
- [9] O. Dreyer, B. J. Kelly, B. Krishnan, L. S. Finn, D. Garrison, and R. Lopez-Aleman, Class. Quant. Grav. 21, 787 (2004), arXiv:gr-qc/0309007.
- [10] S. L. Detweiler, Astrophys. J. **239**, 292 (1980).
- [11] E. Berti, V. Cardoso, and C. M. Will, Phys. Rev. D 73, 064030 (2006), arXiv:gr-qc/0512160.
- [12] S. Gossan, J. Veitch, and B. S. Sathyaprakash, Phys. Rev. D 85, 124056 (2012), arXiv:1111.5819 [gr-qc].
- [13] R. Abbott *et al.* (LIGO Scientific, VIRGO, KAGRA), (2021), arXiv:2112.06861 [gr-qc].
- [14] E. Berti et al., Class. Quant. Grav. 32, 243001 (2015), arXiv:1501.07274 [gr-qc].
- [15] E. Berti, K. Yagi, H. Yang, and N. Yunes, Gen. Rel. Grav. 50, 49 (2018), arXiv:1801.03587 [gr-qc].
- [16] V. Cardoso and P. Pani, Living Rev. Rel. 22, 4 (2019), arXiv:1904.05363 [gr-qc].
- [17] M. Colpi et al. (LISA), (2024), arXiv:2402.07571 [astro-ph.CO].
- [18] M. Maggiore et al. (ET), JCAP 03, 050 (2020), arXiv:1912.02622 [astro-ph.CO].
- $[19] \ \ V. \ \ Kalogera\ \ et\ \ al.,\ \ (2021),\ arXiv:2111.06990\ \ [gr-qc].$
- [20] S. Hild et al., Class. Quant. Grav. 28, 094013 (2011), arXiv:1012.0908 [gr-qc].
- [21] M. Branchesi et al., JCAP ${\bf 07}$, 068 (2023), arXiv:2303.15923 [gr-qc].
- [22] A. Abac et al., (2025), arXiv:2503.12263 [gr-qc].
- [23] B. P. Abbott et al. (LIGO Scientific), Class. Quant. Grav. 34, 044001 (2017), arXiv:1607.08697 [astro-ph.IM].
- [24] R. Essick, S. Vitale, and M. Evans, Phys. Rev. D 96, 084004 (2017), arXiv:1708.06843 [gr-qc].
- [25] M. Evans et al., (2023), arXiv:2306.13745 [astro-ph.IM].
- [26] E. Berti, A. Sesana, E. Barausse, V. Cardoso, and K. Belczynski, Phys. Rev. Lett. 117, 101102 (2016), arXiv:1605.09286 [gr-qc].
- [27] S. Bhagwat, C. Pacilio, E. Barausse, and P. Pani, Phys. Rev. D 105, 124063 (2022), arXiv:2201.00023 [gr-qc].
- [28] S. Bhagwat, C. Pacilio, P. Pani, and M. Mapelli, Phys. Rev. D 108, 043019 (2023), arXiv:2304.02283 [gr-qc].
- [29] C. V. Vishveshwara, Nature 227, 936 (1970).
- [30] K. D. Kokkotas and B. G. Schmidt, Living Rev. Rel. 2, 2 (1999), arXiv:gr-qc/9909058.
- [31] E. Berti, V. Cardoso, and A. O. Starinets, Class. Quant. Grav. 26, 163001 (2009), arXiv:0905.2975 [gr-qc].
- [32] R. A. Konoplya and A. Zhidenko, Rev. Mod. Phys. 83, 793 (2011), arXiv:1102.4014 [gr-qc].

- [33] M. Isi, M. Giesler, W. M. Farr, M. A. Scheel, and S. A. Teukolsky, Phys. Rev. Lett. 123, 111102 (2019), arXiv:1905.00869 [gr-qc].
- [34] N. Franchini and S. H. Völkel, (2023), arXiv:2305.01696 [gr-qc].
- [35] E. Maggio, L. Buoninfante, A. Mazumdar, and P. Pani, Phys. Rev. D 102, 064053 (2020), arXiv:2006.14628 [gr-qc].
- [36] E. Maggio, P. Pani, and G. Raposo, (2021), arXiv:2105.06410 [gr-qc].
- [37] E. Maggio, Lect. Notes Phys. 1017, 333 (2023), arXiv:2310.07368 [gr-qc].
- [38] E. Barausse, V. Cardoso, and P. Pani, Phys. Rev. D 89, 104059 (2014), arXiv:1404.7149 [gr-qc].
- [39] V. Cardoso, K. Destounis, F. Duque, R. P. Macedo, and A. Maselli, Phys. Rev. D 105, L061501 (2022), arXiv:2109.00005 [gr-qc].
- [40] V. Cardoso, K. Destounis, F. Duque,
 R. Panosso Macedo, and A. Maselli, Phys. Rev.
 Lett. 129, 241103 (2022), arXiv:2210.01133 [gr-qc].
- [41] K. Destounis, A. Kulathingal, K. D. Kokkotas, and G. O. Papadopoulos, Phys. Rev. D 107, 084027 (2023), arXiv:2210.09357 [gr-qc].
- [42] E. Barausse, V. Cardoso, and P. Pani, J. Phys. Conf. Ser. 610, 012044 (2015), arXiv:1404.7140 [astro-ph.CO].
- [43] M. H.-Y. Cheung, K. Destounis, R. P. Macedo, E. Berti, and V. Cardoso, Phys. Rev. Lett. 128, 111103 (2022), arXiv:2111.05415 [gr-qc].
- [44] E. Berti, V. Cardoso, M. H.-Y. Cheung, F. Di Filippo, F. Duque, P. Martens, and S. Mukohyama, Phys. Rev. D 106, 084011 (2022), arXiv:2205.08547 [gr-qc].
- [45] S. Biswas, C. Singha, and S. Chakraborty, Phys. Rev. D 109, 064043 (2024), arXiv:2307.04836 [gr-qc].
- [46] C. Singha and S. Biswas, Phys. Rev. D 109, 024043 (2024), arXiv:2309.01760 [gr-qc].
- [47] V. Cardoso, E. Franzin, and P. Pani, Phys. Rev. Lett. 116, 171101 (2016), [Erratum: Phys.Rev.Lett. 117, 089902 (2016)], arXiv:1602.07309 [gr-qc].
- [48] V. Cardoso, S. Hopper, C. F. B. Macedo, C. Palenzuela, and P. Pani, Phys. Rev. D 94, 084031 (2016), arXiv:1608.08637 [gr-qc].
- [49] V. Cardoso and P. Pani, Nature Astron. 1, 586 (2017), arXiv:1709.01525 [gr-qc].
- [50] J. Abedi, N. Afshordi, N. Oshita, and Q. Wang, Universe 6, 43 (2020), arXiv:2001.09553 [gr-qc].
- [51] H.-P. Nollert, Phys. Rev. D 53, 4397 (1996), arXiv:gr-qc/9602032.
- [52] R. G. Daghigh, M. D. Green, and J. C. Morey, Phys. Rev. D 101, 104009 (2020), arXiv:2002.07251 [gr-qc].
- [53] J. L. Jaramillo, R. Panosso Macedo, and L. Al Sheikh, Phys. Rev. X 11, 031003 (2021), arXiv:2004.06434 [gr-qc].
- [54] K. Destounis, R. P. Macedo, E. Berti, V. Cardoso, and J. L. Jaramillo, Phys. Rev. D 104, 084091 (2021), arXiv:2107.09673 [gr-qc].
- [55] E. Gasperin and J. L. Jaramillo, Class. Quant. Grav. 39, 115010 (2022), arXiv:2107.12865 [gr-qc].
- [56] V. Boyanov, K. Destounis, R. Panosso Macedo, V. Cardoso, and J. L. Jaramillo, Phys. Rev. D 107, 064012 (2023), arXiv:2209.12950 [gr-qc].

- [57] J. L. Jaramillo, Class. Quant. Grav. 39, 217002 (2022), arXiv:2206.08025 [gr-qc].
- [58] S. Sarkar, M. Rahman, and S. Chakraborty, Phys. Rev. D 108, 104002 (2023), arXiv:2304.06829 [gr-qc].
- [59] K. Destounis, V. Boyanov, and R. Panosso Macedo, Phys. Rev. D 109, 044023 (2024), arXiv:2312.11630 [gr-qc].
- [60] D. Areán, D. G. Fariña, and K. Landsteiner, JHEP 12, 187 (2023), arXiv:2307.08751 [hep-th].
- [61] B. Cownden, C. Pantelidou, and M. Zilhão, (2023), arXiv:2312.08352 [gr-qc].
- [62] K. Destounis and F. Duque (2023) arXiv:2308.16227 [gr-qc].
- [63] A. Courty, K. Destounis, and P. Pani, Phys. Rev. D 108, 104027 (2023), arXiv:2307.11155 [gr-qc].
- [64] V. Boyanov, V. Cardoso, K. Destounis, J. L. Jaramillo, and R. Panosso Macedo, Phys. Rev. D 109, 064068 (2024), arXiv:2312.11998 [gr-qc].
- [65] L.-M. Cao, J.-N. Chen, L.-B. Wu, L. Xie, and Y.-S. Zhou, (2024), arXiv:2401.09907 [gr-qc].
- [66] V. Cardoso, S. Kastha, and R. Panosso Macedo, Phys. Rev. D 110, 024016 (2024), arXiv:2404.01374 [gr-qc].
- [67] A. Ianniccari, A. J. Iovino, A. Kehagias, P. Pani, G. Perna, D. Perrone, and A. Riotto, Phys. Rev. Lett. 133, 211401 (2024), arXiv:2407.20144 [gr-qc].
- [68] R.-G. Cai, L.-M. Cao, J.-N. Chen, Z.-K. Guo, L.-B. Wu, and Y.-S. Zhou, (2025), arXiv:2501.02522 [gr-qc].
- [69] R. J. Gleiser, C. O. Nicasio, R. H. Price, and J. Pullin, Class. Quant. Grav. 13, L117 (1996), arXiv:gr-qc/9510049.
- [70] R. J. Gleiser, C. O. Nicasio, R. H. Price, and J. Pullin, Phys. Rept. 325, 41 (2000), arXiv:gr-qc/9807077.
- [71] K. Ioka and H. Nakano, Phys. Rev. D 76, 061503 (2007), arXiv:0704.3467 [astro-ph].
- [72] H. Nakano and K. Ioka, Phys. Rev. D 76, 084007 (2007), arXiv:0708.0450 [gr-qc].
- [73] D. Brizuela, J. M. Martin-Garcia, and M. Tiglio, Phys. Rev. D 80, 024021 (2009), arXiv:0903.1134 [gr-qc].
- [74] E. Pazos, D. Brizuela, J. M. Martin-Garcia, and M. Tiglio, Phys. Rev. D 82, 104028 (2010), arXiv:1009.4665 [gr-qc].
- [75] J. L. Ripley, N. Loutrel, E. Giorgi, and F. Pretorius, Phys. Rev. D 103, 104018 (2021), arXiv:2010.00162 [gr-qc].
- [76] N. Loutrel, J. L. Ripley, E. Giorgi, and F. Pretorius, Phys. Rev. D 103, 104017 (2021), arXiv:2008.11770 [gr-qc].
- [77] L. Sberna, P. Bosch, W. E. East, S. R. Green, and L. Lehner, Phys. Rev. D 105, 064046 (2022), arXiv:2112.11168 [gr-qc].
- [78] M. H.-Y. Cheung et al., Phys. Rev. Lett. 130, 081401 (2023), arXiv:2208.07374 [gr-qc].
- [79] K. Mitman et al., Phys. Rev. Lett. 130, 081402 (2023), arXiv:2208.07380 [gr-qc].
- [80] A. Kehagias, D. Perrone, A. Riotto, and F. Riva, Phys. Rev. D 108, L021501 (2023), arXiv:2301.09345 [gr-qc].
- [81] D. Perrone, T. Barreira, A. Kehagias, and A. Riotto, Nucl. Phys. B 999, 116432 (2024), arXiv:2308.15886 [gr-qc].
- [82] M. H.-Y. Cheung, E. Berti, V. Baibhav, and R. Cotesta, Phys. Rev. D 109, 044069 (2024), [Erratum: Phys.Rev.D 110, 049902 (2024)], arXiv:2310.04489 [gr-qc].

- [83] J. Redondo-Yuste, D. Pereñiguez, and V. Cardoso, Phys. Rev. D 109, 044048 (2024), arXiv:2312.04633 [gr-qc].
- [84] J. Redondo-Yuste, G. Carullo, J. L. Ripley, E. Berti, and V. Cardoso, Phys. Rev. D 109, L101503 (2024), arXiv:2308.14796 [gr-qc].
- [85] S. Yi, A. Kuntz, E. Barausse, E. Berti, M. H.-Y. Cheung, K. Kritos, and A. Maselli, Phys. Rev. D 109, 124029 (2024), arXiv:2403.09767 [gr-qc].
- [86] H. Zhu et al., Phys. Rev. D 110, 124028 (2024), arXiv:2404.12424 [gr-qc].
- [87] H. Zhu et al., Phys. Rev. D 109, 104050 (2024), arXiv:2401.00805 [gr-qc].
- [88] M. Giesler, M. Isi, M. A. Scheel, and S. Teukolsky, Phys. Rev. X 9, 041060 (2019), arXiv:1903.08284 [gr-qc].
- [89] S. Bhagwat, X. J. Forteza, P. Pani, and V. Ferrari, Phys. Rev. D 101, 044033 (2020), arXiv:1910.08708 [gr-qc].
- [90] V. Baibhav, M. H.-Y. Cheung, E. Berti, V. Cardoso, G. Carullo, R. Cotesta, W. Del Pozzo, and F. Duque, Phys. Rev. D 108, 104020 (2023), arXiv:2302.03050 [gr-qc].
- [91] R. H. Price, Phys. Rev. D 5, 2439 (1972).
- [92] C. Gundlach, R. H. Price, and J. Pullin, Phys. Rev. D 49, 883 (1994), arXiv:gr-qc/9307009.
- [93] L. Barack, Phys. Rev. D 59, 044017 (1999), arXiv:gr-qc/9811028.
- [94] M. De Amicis, S. Albanesi, and G. Carullo, Phys. Rev. D 110, 104005 (2024), arXiv:2406.17018 [gr-qc].
- [95] M. De Amicis et al., (2024), arXiv:2412.06887 [gr-qc].
- [96] R. F. Rosato and P. Pani, Phys. Rev. D 112, 024080 (2025), arXiv:2505.08877 [gr-qc].
- [97] N. Oshita, JCAP 04, 013 (2023), arXiv:2208.02923 [gr-qc].
- [98] N. Oshita, Phys. Rev. D 109, 104028 (2024), arXiv:2309.05725 [gr-qc].
- [99] K. Okabayashi and N. Oshita, (2024), arXiv:2403.17487 [gr-qc].
- [100] S. W. Hawking, Commun. Math. Phys. 43, 199 (1975),[Erratum: Commun.Math.Phys. 46, 206 (1976)].
- [101] R. F. Rosato, K. Destounis, and P. Pani, Phys. Rev. D 110, L121501 (2024), arXiv:2406.01692 [gr-qc].
- [102] N. Oshita, K. Takahashi, and S. Mukohyama, Phys. Rev. D 110, 084070 (2024), arXiv:2406.04525 [gr-qc].
- [103] C. Bambi et al. (2025) arXiv:2505.09014 [gr-qc].
- [104] Z. Mark, A. Zimmerman, S. M. Du, and Y. Chen, Phys. Rev. D 96, 084002 (2017), arXiv:1706.06155 [gr-qc].
- [105] E. Maggio, P. Pani, and V. Ferrari, Phys. Rev. D 96, 104047 (2017), arXiv:1703.03696 [gr-qc].
- [106] J. Abedi, H. Dykaar, and N. Afshordi, Phys. Rev. D 96, 082004 (2017), arXiv:1612.00266 [gr-qc].
- [107] M. Visser, Lorentzian wormholes: From Einstein to Hawking (1995).
- [108] N. Oshita, Q. Wang, and N. Afshordi, JCAP 04, 016 (2020), arXiv:1905.00464 [hep-th].
- [109] E. W. Leaver, Phys. Rev. D 34, 384 (1986).
- [110] E. Berti and V. Cardoso, Phys. Rev. D 74, 104020 (2006), arXiv:gr-qc/0605118.
- [111] H. O. Silva, G. Tambalo, K. Glampedakis, K. Yagi, and J. Steinhoff, Phys. Rev. D 110, 024042 (2024), arXiv:2404.11110 [gr-qc].
- [112] M. Mirbabayi, JCAP **01**, 052 (2020), arXiv:1807.04843 [gr-qc].

- [113] K. Kyutoku, H. Motohashi, and T. Tanaka, Phys. Rev. D 107, 044012 (2023), arXiv:2206.00671 [gr-qc].
- [114] K. Destounis, M. Malato Corrêa, C. F. B. Macedo, and R. Panosso Macedo, (2025), arXiv:2509.16310 [gr-qc].
- [115] R. F. Rosato, S. Biswas, S. Chakraborty, and P. Pani, Phys. Rev. D 111, 084051 (2025), arXiv:2501.16433 [gr-qc].
- [116] V. Cardoso, L. C. B. Crispino, C. F. B. Macedo, H. Okawa, and P. Pani, Phys. Rev. D 90, 044069 (2014), arXiv:1406.5510 [gr-qc].
- [117] P. Bueno, P. A. Cano, F. Goelen, T. Hertog, and B. Vercnocke, Physical Review D 97 (2018), 10.1103/physrevd.97.024040.
- [118] S. Chakraborty, E. Maggio, A. Mazumdar, and P. Pani, Phys. Rev. D 106, 024041 (2022), arXiv:2202.09111 [gr-qc].

- [119] A. A. Starobinskil and S. M. Churilov, Sov. Phys. JETP 65, 1 (1974).
- [120] E. Maggio, V. Cardoso, S. R. Dolan, and P. Pani, Phys. Rev. D 99, 064007 (2019), arXiv:1807.08840 [gr-qc].
- [121] R. A. Konoplya and A. Zhidenko, JCAP 12, 043 (2016), arXiv:1606.00517 [gr-qc].
- [122] N. Oshita, E. Berti, and V. Cardoso, Phys. Rev. Lett. 135, 031401 (2025), arXiv:2503.21276 [gr-qc].
- [123] A. Maselli, S. H. Völkel, and K. D. Kokkotas, Phys. Rev. D **96**, 064045 (2017), arXiv:1708.02217 [gr-qc].
- [124] P. Pani, Int. J. Mod. Phys. A 28, 1340018 (2013), arXiv:1305.6759 [gr-qc].
- [125] R. Brito, V. Cardoso, and P. Pani, Lect. Notes Phys. 906, pp.1 (2015), arXiv:1501.06570 [gr-qc].